Journal of Applied Fluid Mechanics, Vol. 11, No. 2, pp. 375-384, 2018.
Available online at www.jafmonline.net, ISSN 1735-3572, EISSN 1735-3645.
DOI: 10.29252/jafm.11.02.28185

Characterization of Disturbed Hemodynamics due to Stenosed Aortic Jets with a Lagrangian Coherent Structures Technique

A. B. Olcay[1], A. Amindari[2], K. Kirkkopru[2] and H. C. Yalcin[3†]

[1] *Yeditepe University, Mechanical Engineering Department, Atasehir, Istanbul, 34755, Turkey*
[2] *Istanbul Technical University, Mechanical Engineering Department, Istanbul, Turkey*
[3] *Qatar University, Biomedical Research Center, PO Box 2713, Doha, Qatar*

†*Corresponding Author Email: hyalcin@qu.edu.qa*

(Received July 6, 2017; accepted November 21, 2017)

ABSTRACT

The aortic valve is located at left ventricular outlet and is exposed to the highest pressure in the cardiovascular system. Problems associated with the valve leaflet movement can cause complications for the heart. Specifically, aortic stenosis (AS) arises when aortic leaflets do not efficiently open. In the present study, Lagrangian Coherent Structures (LCSs) were utilized by processing a variety of Computational Fluid Dynamics (CFD) models velocity vector data further to identify the characteristics of AS jets. Particularly, effective orifice areas (EOA) for different cases were accurately identified from unstable manifolds of finite time Lyapunov exponent (FTLE) fields. Calcified leaflets were modeled by setting the leaflet's Young modulus to 10 MPa and 20 MPa for moderately and severely calcified leaflets respectively while a healthy leaflet's Young modulus was assigned to be 2 MPa. Increase in calcification degree of the leaflet caused destruction of the vortex structures near the fibrosa layer of the leaflet indicating a malfunctioning for the movement mechanism of the leaflet. Furthermore, when we analyzed stable manifolds, we identified a blockage region at the flow upstream due to the stagnant blood here. Compared to a healthy case, for the calcified valve, this blockage region was enlarged, implying an increase in AS jet velocity and wall shear stress on leaflets. As a conclusion, results from the present study indicate that aortic leaflet malfunctioning could be accurately evaluated when LCS technique was employed by post processing velocity vector data from CFD. Such precise analysis is not possible using the Eulerian CFD approach or a Doppler echocardiography since these methods are based on only analyzing instantaneous flow quantities and they overlook fluid flow characteristics of highly unsteady flows.

Keywords: Lagrangian coherent structures; Aortic valve; Stenosis; Computational fluid dynamics; Fluid structure interaction; Calcification; Hemodynamics; Vortex; Wall shear stress; Pressure.

1. INTRODUCTION

The aortic valve sits at the inlet of the aorta and regulates blood flow exiting from the left ventricle. It consists of three leaflets within the aortic sinuses. A healthy valve fully opens at ventricular systole and closes at ventricular diastole ensuring unidirectional blood flow with minimal regurgitation. Calcification is the most common aortic valve disease affecting mainly the elderly, with an incidence rate of 2-7% above age 65 (Stewart, Siscovick *et al*. 1997). Calcified leaflets cannot efficiently open at peak flow which results in aortic stenosis (AS). AS is the formation of high velocity jet at the valve orifice. Identification of this high velocity jet is an indication of valve calcification and hence used to diagnose this condition. Doppler echocardiography is the most commonly used technique for that purpose. Doppler can measure the maximum blood velocity at the valve orifice, but not the axial velocity profile of the jet (DeGroff 2002). The assumption of constant velocity along the jet orifice will lead to some potential errors in further calculations. The effective orifice area (EOA) is another parameter used by physicians for the clinical assessment of AS severity. EOA is the minimal cross sectional area of the aortic flow jet. EOA can be calculated from a continuity equation by relating Doppler measured velocities at the aortic valve inlet and jet orifice. Due to simplifying assumptions and inaccuracy of the measurements, calculating EOA from Doppler velocities were shown to be associated with significant errors (DeGroff 2002, Baumgartner

2006, Shadden, Astorino *et al*. 2010).

Accurate diagnosis of the severity of aortic disease is crucial for therapy planning. However, as explained above, current approaches are associated with significant errors in hemodynamic analysis. Computational fluid dynamics (CFD) modeling has emerged as an alternative approach for elucidating complex cardiovascular flows where clinical measurement schemes would provide only limited information. There are numerous previous numerical studies on aortic valve hemodynamics (Weinberg, Schoen *et al.* 2009, Mei, de Souza Junior *et al.* 2016, Youssefi, Gomez *et al.* 2017). Aortic valve behavior is a complex dynamic event since it involves both fluid and structure movements. To model this complex dynamic problem, the fluid-structure interaction (FSI) approach should be adapted. In this approach, valve leaflets are modeled as a deformable structural domain and blood flow is modeled as a fluid domain. Two domains are coupled and mathematical solutions of the fields are determined simultaneously (Chandra, Rajamannan *et al*. 2012, Kuan and Espino 2015, Pan, Qiao *et al*. 2015). We have recently developed a methodology to model aortic valve hemodynamics using the commercial software package program ANSYS. Details of this approach is explained elsewhere (Amindari and Yalcin 2014, Amindari and Yalcin 2015).

In flow analysis, Eulerian and Lagrangian approaches play an integral role in understanding fluid flow characteristics. In particular, instantaneous velocity vector data can be obtained for a region of interest by utilizing CFD analysis and/or employing the digital particle image velocimetry (DPIV) method. Therefore, Eulerian methodology provides instantaneous velocity vector data for selected regions of interest. Obtaining flow fields alone is not sufficient to investigate highly transient problems such as complex biological flows. For example, Eulerian method can present blood velocity vector information at each point in the area of interest for fluid flow through an aortic valve; however, the position variation of a leaflet cannot be monitored in this technique. Therefore, while the Eulerian approach is able to monitor instantaneous fluid flow values in a certain region, an overall analysis of the flow is not quite possible. In the Lagrangian approach; on the other hand, velocity vectors obtained from CFD or DPIV are integrated in forward and backward directions to identify finite time Lyapunov exponent (FTLE) fields. The mathematics behind FTLE analysis was comprehensively discussed by Shadden *et al.* (Shadden, Lekien *et al*. 2005). For instance, a bifurcation region of a cardiovascular fluid flow was simplified in a CFD model and FTLE fields were obtained to reveal the boundaries of a forming vortex (Shadden and Taylor 2008, Vétel, Garon *et al*. 2009). Furthermore, the high velocity jet appearing during systole causes the formation of vortex structures behind the aortic valves. These vortex structures play important roles in blood mass transportation, leaflet's oscillation and wall shear stress (WSS) magnitude on fibrosa surface of the leaflet (i.e., back surface of the leaflet). Flow separation and mixing zones of fluid flow were also determined by the results of FTLE analysis. The Lagrangian Coherent Structures (LCS) technique utilized in the present study has been previously used to investigate the dynamics of transient jet flows, vortex formations and turbulence (Haller and Yuan 2000, Chrisohoides and Sotiropoulos 2003, Olcay and Krueger 2008, Shadden and Taylor 2008, Vétel, Garon *et al.* 2009, Olcay and Krueger 2010, Töger, Kanski *et al*. 2012, Olcay 2016). In this technique, since results from the Eulerian analysis are utilized by the Lagrangian approach, particles` initial and intermediate locations along with the particle paths can be tracked. Shadden *et al.* studied a simplified two-dimensional CFD model to understand fluid flow characteristics of a jet across an aortic valve (Shadden, Astorino *et al.* 2010). Aortic aneurysm flows, which are among the most complex fluid flows, can also be examined with FTLE fields. For example, Shadden and Arzani recently emphasized the complexity of the blood flow in the heart and in large vessels and pointed out the significance of the Lagrangian based post-processing technique (Shadden and Arzani 2015). They also showed that when this technique is employed for aneurysms originating in an aortic vessel, vortex structure formed in the aneurysm can be identified with FTLE fields. As a result, FTLE fields have been started to be adapted in studies on complex biological fluid flows.

In the present study, the results of a variety of numerical aortic valve models were post processed to compute FTLE fields. Identification of LCSs from FTLE fields provided better understanding of the aortic leaflet movement mechanism than the Eulerarian approach's instantaneous velocity vector data. Particularly, LCSs were utilized to determine jet flow characteristics near ventricularis surfaces and movement of vortex structures near the fibrosa surfaces for healthy and calcified valve leaflets. In addition to analyzing flow characteristics, we were able to show that diagnosis parameters such as EOA could be precisely determined via LCS technique.

2. MATERIALS AND METHODS

Aortic valve hemodynamics of a calcified leaflet was simulated using CFD method (Amindari *et al.* 2017); however, numerical methods employed into fluid flow domain is discussed here for completeness of the present study. Velocity vectors obtained from CFD analysis were further processed with LCS technique to investigate the jet dynamics around the leaflets.

2.1 Numerical Model

A 2D model geometry was created in Design Modeler module of Ansys Workbench using b-mode echocardiography images of a patient`s aortic valve (Fig. 1(a)). While ventricularis and fibrosa surfaces of the leaflet were identified in Fig. 1(a), deformable dynamic mesh was utilized for the leaflet as shown in Fig. 1(b). As the 2D model geometry possessed both fluid flow region and

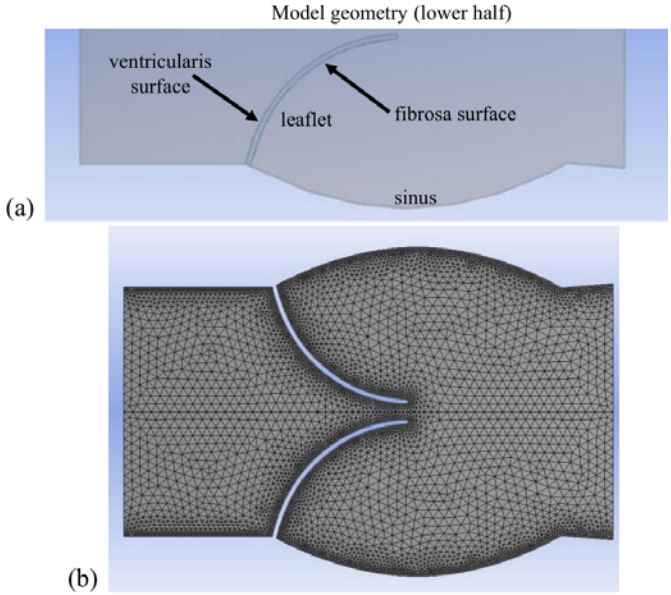

Fig. 1. Numerical model geometry showing leaflet's ventricularis and fibrosa surfaces (a); Deformable dynamic structural mesh is placed into the meshed fluid zone (b).

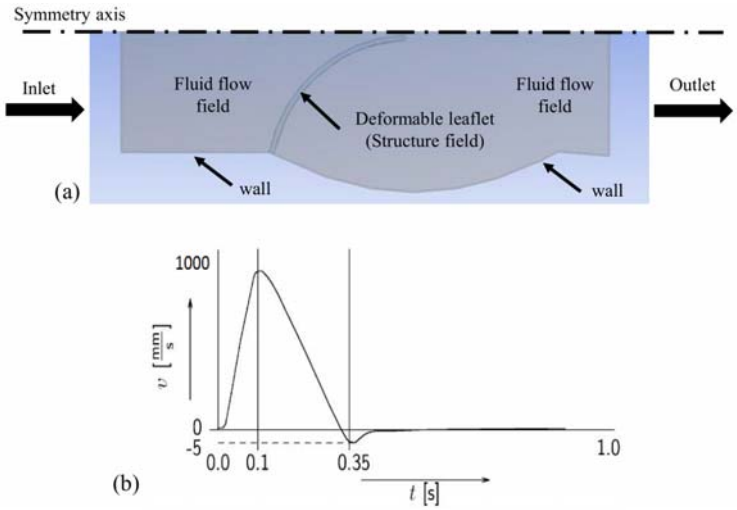

Fig. 2. Numerical model geometry with boundary conditions (a); Patient specific measured velocity profile (b).

leaflets' structure, the fluid flow and structure fields were created to simulate fluid flow across the aortic valve as illustrated Fig. 2(a). Specifically, fluid structure interaction (FSI) was employed for the leaflet surfaces so that blood flow would be able to deform the leaflet forward or backward depending on the pressure variation across the valve. While the lower edge of the geometry was chosen to be a rigid wall with no slip as shown in Fig. 2(a), the left edge, also named the aortic valve inlet, of the numerical model was set to be a velocity inlet. Doppler echocardiography velocities from a patient`s aortic valve were employed for this edge as a transient velocity boundary condition as illustrated in Fig. 2(b). These velocity data were implemented as a user defined function (UDF) for the numerical model. The right edge of the model was defined to be a pressure outlet with a zero gage pressure.

Both fluid and solid zones of the numerical model were discretized to solve the velocity and pressure variations over the aortic valve. Mesh convergence tests were performed for the numerical model at the peak steady state velocity by increasing the number of elements and monitoring the key parameters of fluid flow to determine the required number of elements of the numerical model with reasonable accuracy. It was observed that use of nearly 10,000 elements for fluid zone provided reasonable accuracy. Therefore, 10,000 hexahedral and tetrahedral elements were placed for the fluid region using the sweep method. To capture the high velocity gradients at structure surfaces, a higher density mesh was utilized for the near rigid walls and leaflets surfaces. For an accurate and low cost

capture of the leaflet deformations, a high quality mesh with 77 uniform tetrahedral elements were employed to the structure zone (Fig. 1(b)).

Ansys Fluent was employed to solve governing equations of the fluid flow region while Ansys transient structural module was utilized to simulate the dynamic response of leaflets for time-dependent blood flow forces. Behavior of the blood in the fluid domain was assumed to be Newtonian and the blood's density and dynamic viscosity were taken to be 1060 kg/m^3 and 0.0035578 Pa.s, respectively. Realizable k-ε turbulence model was employed to capture fluid flow behavior around the leaflet and recirculatory flows at the downstream of the valve. On the other hand, transient forces, displacements, deformations, strains and stresses on the leaflets were obtained solving an equation of motion. An isotropic linear elastic material was defined for leaflets and leaflets' density was set to 1060 kg/m^3 to eliminate any buoyancy effects in the computational model (Maleki, Shahriari *et al.* 2014). In the present study, modulus of elasticity of 2 MPa was used for healthy leaflets (Gnyaneshwar, Kumar *et al.* 2002) while modulus of elasticity of 10 MPa and 20 MPa (Acton 2012) were utilized for moderately and severely calcified leaflets, respectively (Amindari and Yalcin 2015). Leaflets' possion ratio was taken to be 0.3 (Gnyaneshwar, Kumar *et al.* 2002).

The blood fluid zone was coupled with leaflet structure using the FSI approach. This was achieved with an iterative implicit 2-way coupling technique so that blood flow data and movement of the aortic valve leaflets data were communicated with each other. In this technique, fluid flow and structural zones are solved separately by Ansys Fluent and Ansys Mechanical APDL, respectively. Ansys Fluent is based on a finite volume method whereas Ansys Mechanical APDL is based on a finite element method. Furthermore, the system coupling module is capable of transferring information such as pressure data from fluid zone to the structural side. Similarly, displacement data due to pressure applied on leaflets is transferred back to the fluid flow region to update the fluid zone mesh for each time point. Cardiac cycle time was divided into time steps and each time step required several iterations to perform fluid flow and structural zone calculations. Time step size of 6e-5 seconds and maximum coupling iterations limit of 5 were used for an implicit scheme because these values provided enhanced solution stability.

2.2 Lagrangian Coherent Structures (LCS)

Once velocity vector calculations were completed using the FSI model, flow dynamics across the leaflets was investigated by LCS. Details of the LCS approach is provided by Shadden *et al.* (Shadden, Lekien *et al.* 2005); however, the LCS technique was briefly discussed here to explain how FTLE fields were obtained for the completeness of the study. The path of a fluid particle at location at time can be expressed as

$$\dot{\mathbf{x}}(t;t_0,\mathbf{x}_0)=\mathbf{V}(\mathbf{x}(t;t_0,\mathbf{x}_0),t) \tag{1}$$

In here, $\mathbf{x}(t_0;t_0,\mathbf{x}_0)=\mathbf{x}_0$ and the right side of the Eq (1) represent either experimental or numerical velocity vector data. In the present study, velocity data were obtained from FSI model and the solution of Eq (1) is actually a flow map and can be written as $\varphi_{t_0}^{t_0+T}(\mathbf{x}_0)$. Besides, this flow map defines a fluid particle's position at $t=t_0+T$ and the same particle was actually at $\mathbf{x}_0$ position when $t=t_0$. Therefore, the solution of the flow map can be given as,

$$\phi_{t_0}^{t_0+T}(\mathbf{x}_0)=\mathbf{x}(t_0+T;t_0,\mathbf{x}_0) \tag{2}$$

and FTLE can be expressed as,

$$\sigma_{t_0}^{T}(\mathbf{x})\equiv\frac{1}{|T|}\ln\sqrt{\lambda_{\max}} \tag{3}$$

Here, λ_{max} is the maximum eigenvalue of $\left(\nabla\varphi_{t_0}^{t_0+T}(\mathbf{x})\right)^{*}\left(\nabla\varphi_{t_0}^{t_0+T}(\mathbf{x})\right)$ and $(\,)^{*}$ represents the adjoint operation. Shadden *et al.* also showed that the particle's separation from each other for a given flow field was proportional to $e^{\sigma_{t_0}^{T}(\mathbf{x})|T|}$ (Shadden, Lekien *et al.* 2005). Therefore, FTLE can be seen as a measure of maximum expansion rate of fluid particles in the flow field. The high values in the FTLE field illustrate ridge boundaries and ridges of FTLE fields are defined as LCSs. Furthermore, fluid flow through a LCS scales in the order of $\frac{1}{|T|}$; therefore, LCSs are accepted to be transport barriers or material lines for high $|T|$ values since flow cannot cross these boundaries. Furthermore, LCSs calculated by taking forward and backward time integrations are called stable and unstable manifolds. These manifolds divide the flow domain by material lines so that circulation regions, flow separation points and vortex boundaries can be identified. In the present study, axial and radial velocity components obtained from the FSI model were written in ASCII format for each time step. An in-house-code programmed in Matlab was used to generate a single file containing the entire velocity. However, when cardiac cycle was examined along with the flow's velocity field, it was realized that at only the first half of the cardiac cycle, blood flow was present (valve opening and closure) while the second half of the cardiac cycle blood flow velocities were close to zero over the aortic valve. Therefore, FTLE calculations were performed from 0 seconds to 0.3 seconds for a cardiac cycle of 0.6 seconds. FTLE were determined for every 25th time step which results in a time resolution of 0.0015 seconds. Horizontal and vertical distances of the solution domain were 0 to 0.04 m and 0 to 0.0135 m, respectively. Size of elements in the FTLE fields for both horizontal and vertical directions was set to be 0.5e-5 so that the FTLE fields were obtained with a high resolution of 800 by 270. These calculations were performed for each velocity vector data of FSI

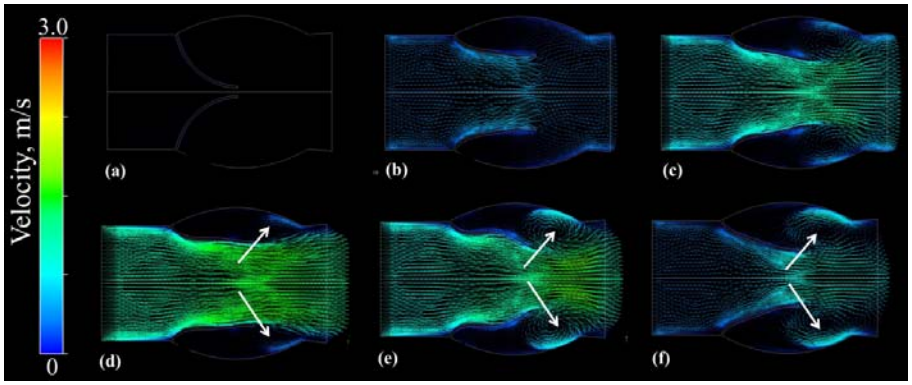

Fig. 3. Time variation of velocity vector field for healthy leaflet model's fluid flow domain. Velocity vector field at t = 0.0015 s (a), Velocity vector field at t = 0.05 s (b), Velocity vector field at t = 0.1 s (c), Velocity vector field at t = 0.15 s (d), Velocity vector field at t = 0.18 s (e), Velocity vector field at t = 0.25 s (f).

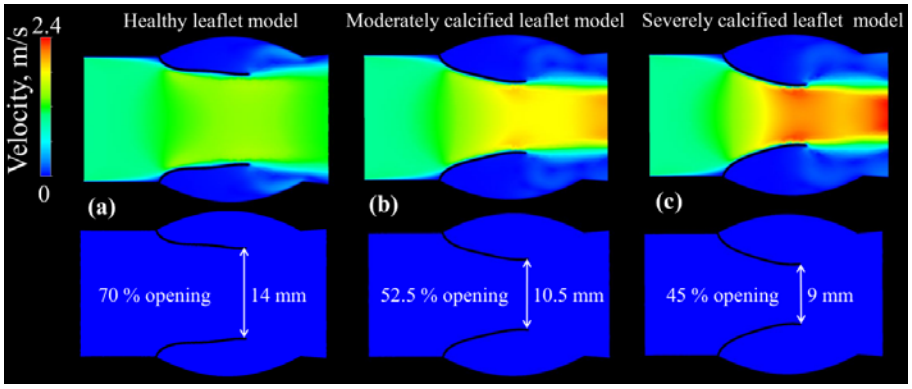

Fig. 4. Velocity contour plots for healthy leaflet model (a); moderately calcified leaflet model (b); severely calcified leaflet model (c).

runs. FTLE calculations were obtained by forward and backward integration from 0 second to 0.3 seconds and from 0.3 seconds to 0 second so that stable and unstable manifolds could be revealed. Due to the symmetry of the geometry about central axis, we calculated LCS for only lower half of the geometry to save computation time.

3. RESULTS AND DISCUSSION

3.1 Fluid Flow Characteristics for the Healthy and Calcified Leaflet Models

Velocity vector field of a healthy leaflet model was shown in Fig. 3 for different time points to provide characteristics of fluid flow domain during a cardiac cycle. Velocity vectors exhibit low values for t < 0.05 s since inlet velocity profile defined for left edge reaches its peak velocity at t = 0.1 s (Fig. 3 (a) and (b)). Then, significant increase in velocity vector magnitudes is seen for later times. Furthermore, circulation regions near leaflet ends marked with white arrows were observed in Fig. 3 (d), (e) and (f) because of flow separation at the leaflet ends.

While a healthy leaflet simulation was performed for a 2 MPa Young modulus leaflet structure, moderately and severely calcification on leaflets were examined by assigning Young modulus of 10 MPa and 20 MPa to the leaflets, respectively. Figures 4 (a), (b) and (c) illustrate velocity contour plots for healthy, moderately and severely calcified leaflets at peak systole, respectively. A parameter named opening ratio was defined by Armin *et al*. 2017, as a percentage of diameter orifice to blood vessel diameter to determine stenosis quantitatively. They documented that opening ratio of severely calcified leaflets was 45% indicating that nearly half of the vessel was not available for blood flow. On the other hand, moderately calcified leaflets' opening ratio was about 53% while healthy leaflets gave 70% opening ratio. When healthy and severely calcified leaflets are compared, it is noted that area of severely calcified leaflets can be reduced nearly half of the healthy leaflets yielding almost two times higher velocity at the smallest area. This can actually directly affect the fluid flow characteristics for the severely calcified leaflets case. Streamlines and velocity vector plots for healthy, moderately and severely calcified leaflets were also obtained at peak systole and given in Figs. 5 (a), (b) and (c). Streamline plots demonstrates a converging type flow for all leaflet models while circulation regions appear all three cases. It is noticed that when calcification degree raises, leaflets' opening ratio becomes smaller causing circulation regions to be larger. This

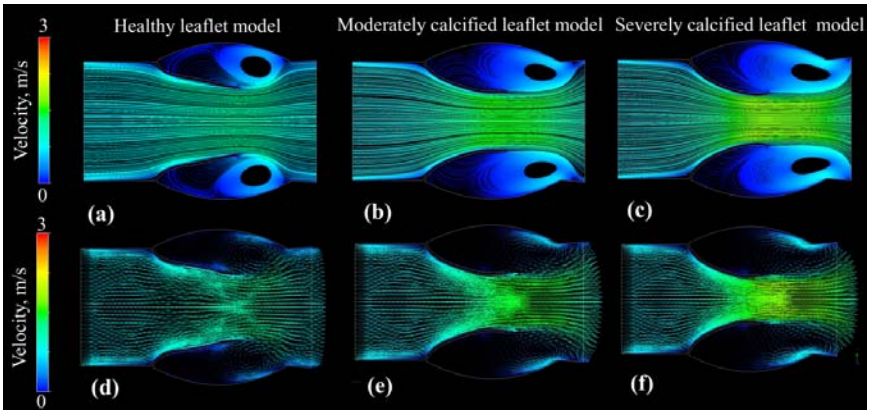

Fig. 5. Velocity streamline contour and velocity vector plots for healthy leaflet model (a); moderately calcified leaflet model (b); severely calcified leaflet model (c).

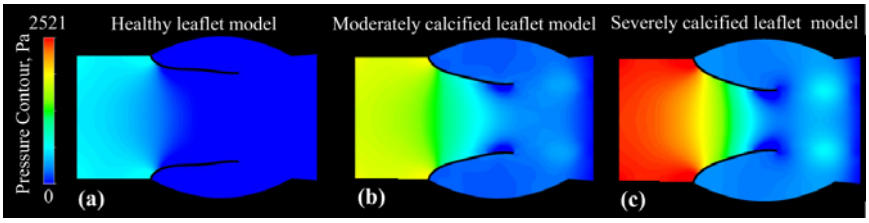

Fig. 6. Pressure contour plots for healthy leaflet model (a); moderately calcified leaflet model (b); severely calcified leaflet model (c).

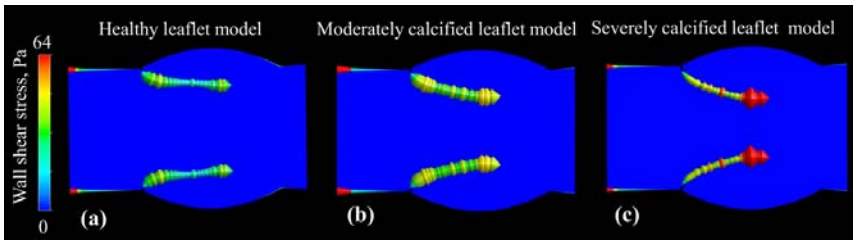

Fig. 7. Wall shear stress contour plots for healthy leaflet model (a); moderately calcified leaflet model (b); severely calcified leaflet model (c).

implies that larger circulation region can result in larger pressure drop undermining the heart performance. Velocity vector plots also agree with opening ratio and indicate that when circulation regions are large, fluid must flow thru a small area. Therefore, fluid's velocity becomes highest at the smallest area to satisfy conservation of mass.

As calcification affect pressure across aortic leaflets as discussed previous paragraph, pressure contour plots were also obtained at peak systole and given for healthy, moderately and severely calcified leaflets in Figs. 6 (a), (b) and (c), respectively. Pressure contour plots are in agreement with streamline and velocity vector figures since largest velocity occurring for severely calcified also causes highest pressure difference across the leaflets. It is also noticed that while pressure drop across a healthy leaflet model is only about 600 Pa, moderately and severely calcified leaflets overloads the heart over 3 and 4 times compared to the healthy leaflet model. Lastly, wall shear stresses (WSS) on leaflets were also evaluated and provided in octahedron representation at peak systole for healthy, moderately and severely calcified leaflets in Figs. 7 (a), (b) and (c), respectively to identify surface wear of leaflets. Since WSS can be seen as a frictional force on leaflets, the high values of WSS can sign a possible thinning or wear on leaflets. It is noticed that WSS of severely calcified leaflets is approximately 2 and 3 times larger than moderately calcified and healthy leaflet, respectively.

Although use of Eulerian approach provided key features of fluid flow such as velocity, streamline, pressure and WSS plots, following sections of the present work were dedicated to Lagrangian approach to evaluate flow domain further.

3.2 Validation of FTLE Results

Use of FTLE field promises to identify material lines of blood flow across the aortic valve; however, to validate our model, we initially compared FTLE data from the present study with previous work. Particularly, Shadden *et al*. investigated a simplified two dimensional leaflet model to obtain LCSs and

they documented FTLE field for their model as shown in Fig. 8(a) (Shadden, Astorino *et al.* 2010). In the present study, the FTLE field obtained from backward integration between 0 and 0.225 seconds is presented in Fig. 8(b). Both FTLE fields employed nearly the same cardiac cycle durations and velocity profiles. Our results showed similar LCSs for flow near ventricularis and fibrosa surfaces implying the present simulation results agree with the previous work. It should be noted that FTLE calculations did not include leaflet structure; however, LCSs in Figs. 8(a) and 8(b) indicate that the leaflet shape was revealed with integration of blood velocity in the solution domain. Furthermore, contour level of 8.5 and 9 shown in Fig. 8(b) as red color lines illustrated the manifolds; similarly, the manifolds of Shadden *et al*. are shown in Fig. 8(a) with dark red lines (Shadden, Astorino *et al.* 2010). Briefly, fluid particles cannot pass through these manifolds (i.e., red lines in the FTLE field) and these lines behave as transport barriers or material lines. Particularly, LCS appeared to be a quarter circle shape at the upstream of the aortic valve shown with a black color arrow in Fig. 8(a) and 8(b). Since the flow cannot cross LCS in the solution domain, the blood flow needs to be significantly accelerated above the LCS (i.e., upper region of the quarter circle shape red line) due to the reduction in cross sectional area in this region. This causes high wall shear stresses on ventricularis surface of the aortic valve since the velocity gradient on the wall is directly associated with the magnitude of a wall shear stress. Besides, LCS seemed to be in an elliptical shape at the downstream of the aortic valve given with a white color arrow in Figs. 8(a) and 2(b). This implies that blood flow creates a recirculation zone below the aortic valve and does not move upstream.

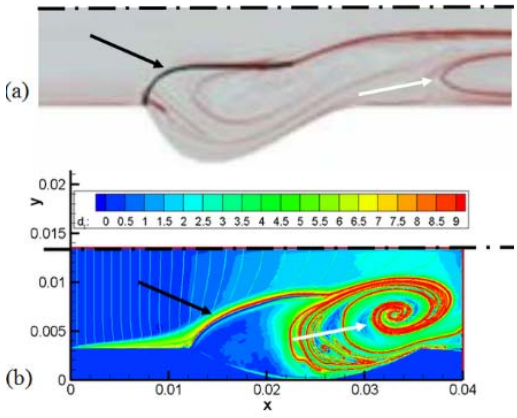

Fig. 8. FTLE field obtained by Shadden *et al.* (2010) (a); FTLE field of the present study from backward integration between 0 and 0.225 seconds (b).

3.3 Effect of Leaflet Calcification on the Stenosis Jet Area with LCS Method

Aortic valves can get calcified with age and calcification of aortic valve leaflets results in increased stiffness. Therefore, blood flow is typically exposed to more resistance to move through calcified aortic valves with high stiffness compared to healthy valves. Besides, calcification formation and growth on aortic valve leaflets result in reduction in the stenosis area. When the area of stenosis becomes smaller, the velocity at this section reaches very high velocities due to mass conservation yielding to a turbulent flow across the leaflet. As a result, a heart may be subjected to additional loads due to the higher pressure requirement of turbulent flow because these types of flows typically cause larger pressure drops. In the present study, aortic valves with three different Young modulus values were investigated to understand the effect of calcification on hemodynamics at the aortic valve. Particularly, Young modulus of 2 MPa, 10 MPa and 20 MPa were used for FSI simulations to mimic the behavior of leaflets with and without calcification. Therefore, leaflets with Young modulus of 10 MPa and 20 MPa represented moderately and severely calcified leaflets while a leaflet with Young modulus of 2 MPa implied a healthy leaflet. Once FSI calculations were completed, velocity vector data were post-processed for FTLE calculations. Fig. 9(a) shows unstable manifolds of a FTLE field of a healthy leaflet obtained from backward integration of velocity data from 0.3 to 0 seconds. Blood flow behind the leaflet seemed to have flow circulation with vortex-like structures since LCS in Fig. 9(a) illustrated an organized circular shape. As the flow cannot cross these circular LCS, there must be flow circulation below the leaflet. This flow circulation probably applies pressure to the fibrosa surface of the leaflet and the leaflet exhibits oscillation during the cardiac cycle. It was also noticed that EOA could be identified to be nearly 2.5 mm. Traditionally, echocardiography is used to determine EOA. However, this technique does not account for the jet flow but solely depends on tracing leaflet tissue. Therefore, use of a FTLE field to identify the EOA provides more accurate EOA since the FTLE method takes into account the blood flow velocities through the cardiac cycle.

In addition to a healthy leaflet simulation, moderately and severely calcified leaflets were examined by assigning Young modulus of 10 MPa and 20 MPa to the leaflets, respectively. Figure 9(b) illustrates unstable manifolds of a FTLE field for an aortic leaflet with a Young modulus of 10 MPa. Flow circulation (i.e., vortex like) zones identified in the FTLE field for the healthy leaflet appeared to be stretched about flow direction for the leaflet with 10 MPa Young modulus (Fig. 9(b)). Specifically, flow circulation balancing leaflet fluctuations seemed to be partially destroyed and bulk of LCS was initially located below the leaflet now to be located at downstream. This would probably affect the movement mechanism of the leaflet and eventually undermine the effectiveness of the leaflet in closing and opening phases. Furthermore, EOA was decreased 20% to nearly 2 mm for the moderately calcified leaflet. This area reduction would cause over 60% velocity increase at the upper portion of the leaflet since velocity is proportional to the square of a diameter. The FTLE field of a severely calcification leaflet is shown in

Fig. 9(c). The vortex structures for the leaflet with 20 MPa Young modulus seemed to be destroyed. This would indicate that the leaflet movement mechanism was almost terminated for 20 MPa Young modulus leaflet because nearly all vortices were totally demolished for this case and leaflet oscillation could not be controlled by the leaflet anymore. This would definitely yield to continuous failure in leaflet functionality and the leaflet could not open and close fully during a cardiac cycle. Furthermore, it was revealed that decrease in EOA of a severely calcified leaflet was about 67% compared to EOA of a healthy leaflet. This area reduction would result in about 280% increase in blood velocity at the upper part of the 20 MPa Young modulus leaflet turning flow regime to a turbulent flow. This increased velocity would also cause very high velocity gradient and WSS on the leaflet's ventricularis surface. High WSS could cause erosion or deformation on the ventricularis surface of the leaflet. As a result, a severely calcified leaflet can be further deformed and cause much larger pressure drop across the valve demanding to compensate this pressure from the heart. The increased load (i.e., high-pressure demand) is associated with heart attack risk.

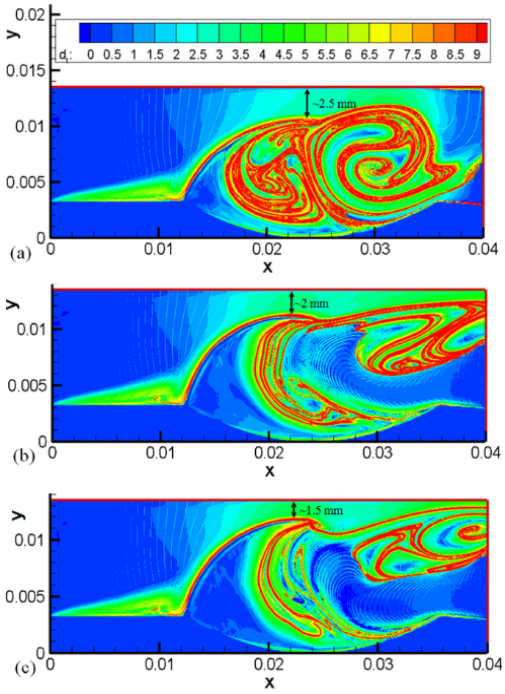

Fig. 9. FTLE fields obtained from unstable manifolds for aortic valve with Young modulus of 2 MPa (a), 10 MPa (b) and 20 MPa (c). Organized vortex structures appear for a healthy leaflet and these structures play an important role for leaflet oscillations during systole (a). Deformed and destroyed vortices are observed for moderately (b) and severely calcified leaflets (c), indicating possible malfunctioning of the leaflet movement. EOA for 2 MPa, 10 MPa and 20 MPa Young modulus leaflets are nearly 2.5 mm, 2 mm and 1.5 mm, respectively.

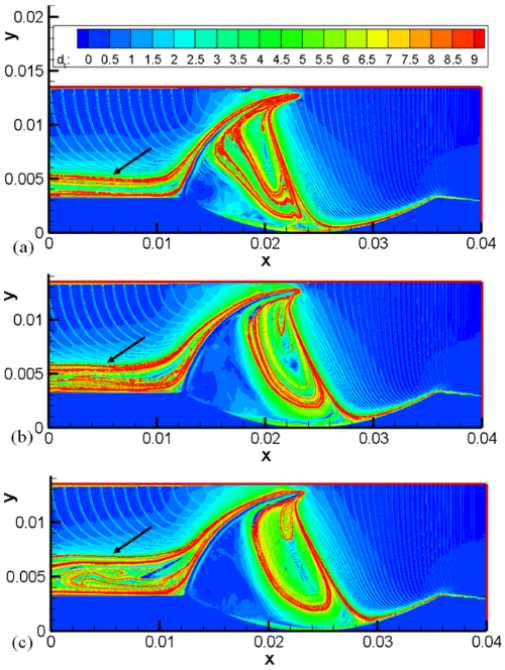

Fig. 10. FTLE fields obtained from stable manifolds for aortic valve with Young modulus of 2 MPa (a), 10 MPa (b) and 20 MPa (c). A large vortex structure covering most of the fibrosa surface of the leaflet is observed for a healthy leaflet and a blockage zone appearing at the upstream is shown with a black arrow. The Vortex structure is seen to be moved to the tip of the leaflet for moderately and severely calcified leaflets implying deterioration of efficient closure mechanisms of the leaflets. Blockage region of moderately and severely calcified leaflets appeared to be thicker compared to the healthy leaflet causing larger blood flow velocities.

3.4 Investigation of Upstream flow Dynamics for Different Leaflet Calcifications

In this section of the present study, stable manifolds of FTLE fields were calculated by forward integration of blood flow velocity data to understand the hemodynamics of upstream blood flow. Similar to the analogy discussed in the previous section, leaflets with Young modulus of 10 MPa and 20 MPa indicated moderate and severe calcification degrees while leaflets with Young modulus of 2 MPa represented a healthy leaflet for stable manifold calculations. Figure 10(a) illustrates stable manifolds for the aortic valve with Young modulus of 2 MPa. It was noticed that LCS seemed to be a rectangular shape identifying a stagnant region marked with a black color arrow at the flow upstream. The height of this rectangular-like structure was nearly 2 mm and this stagnant region occupied about 20% of the total area. Besides, there were LCSs just below the leaflet implying existence of a circulation zone. These LCSs below the leaflet appeared to cover most of the fibrosa surface indicating that leaflet oscillations could be supported with this recirculation region. Figures

10(b) and 10(c) were given to show behavior of stable manifolds for a moderately and severely calcified leaflet, respectively. Nearly 30% of flow upstream (i.e., 3 mm out of 10 mm) was blocked for the leaflet with Young modulus of 10 MPa while the stagnant region was about 40% (i.e., 4 mm out of 10 mm) for the severely calcified leaflet at the upstream. Additional blockage of flow upstream causes higher flow velocities and WSS at the ventricularis surface. Furthermore, LCS structure below the leaflet seemed to be moved to the downstream and it could only support approximately less than half of the leaflet. As a result, calcified leaflets caused stable manifolds to appear at the trailing edge of the leaflet by supporting only a short leaflet piece. This would affect the moving mechanism of the leaflet and possibly would decrease the effectiveness of the aortic leaflet, agreeing to the findings of unstable manifolds.

4. CONCLUSION

Movement of an aortic valve during a cardiac cycle was investigated by CFD and FEA simulations along with FSI analysis. Although CFD - FEA hybrid simulations provided velocity and pressure data at every point in computational domain based on the Eulerian approach, velocity and pressure were not sufficient to completely understand the aortic valve movement and fluid flow behavior around the valve. Velocity data obtained for three different Young modulus values of leaflets were further processed to reveal unstable and stable manifolds via LCS technique. Specifically, the unstable manifolds in FTLE fields of 2 MPa, 10 MPa and 20 MPa revealed hemodynamic behavior across the aortic leaflet by illustrating vortex structures behind the leaflet. It was noted that the healthy leaflet model exhibited a very organized vortex structure near the fibrosa surface of the leaflet supporting the leaflet oscillations during systole. However, these vortex structures appeared to be partially or totally destructed in the LCSs analysis for the moderate and severe calcification leaflet models, respectively. This indicated that the movement of the leaflet would be seriously disturbed for calcified valve leaflets. Furthermore, LCS technique based on unstable manifolds precisely determined the EOA and it was suggested that AS could be diagnosed in a clearer way than the Doppler echocardiography method. Similarly, stable manifolds of FTLE fields identified a blockage in flow upstream and it was noticed that the thickness of this zone was varied based on the degree of calcification on the valve leaflets. When calcification of leaflets was increased, the blockage region filled with stagnant fluid was also enlarged causing higher blood flow at the upstream. LCSs below the aortic leaflet were nearly covering the fibrosa layer of the healthy leaflet yielding to a normal oscillation for the leaflet. However, LCSs of the moderately and severely calcified leaflets were moved to the edge of the leaflet implying that vortex structures were affected by the degree of calcification. As a result, findings of the present study indicated that leaflet malfunctioning could be accurately determined by LCS technique while other methods could only provide instantaneous velocity and pressure data overlooking the fluid flow characteristics.

ACKNOWLEDGEMENTS

This research was supported by a Marie Curie International Reintegration Grant within the 7th European Community Framework Programme (IRG276987 to HCY) and by The Scientific and Technological Research Council of Turkey, TUBITAK (112M148 to HCY and 112M895 to HCY).

REFERENCES

Acton, Q. A. (2012). Heart Valves—Advances in Research and Application, ScholarlyEditions.

Amindari, A. and H. C. Yalcin (2014). Numerical Assessment of Turbulent Flow Downstream of Stenosed Aortic Valve with Flexible Leaflets Using Fluid-Solid Interactions Approach. *Bioinformatics and Bioengineering (BIBE), 2014 IEEE International Conference on*, IEEE.

Amindari, A. and H. C. Yalcin (2015). Numerical investigation of influence of leaflet calcification on aortic valve hemodynamics. *AIP Conference Proceedings* 1648(1), 320005.

Amindari, A., L. Saltik, K. Kirkkopru, M. Yacoub and H. C. Yalcin (2017). Assessment of calcified aortic valve leaflet deformations and blood flow dynamics using fluid-structure interaction modeling. *Informatics in Medicine Unlocked* 9 (Supplement C): 191-199.

Baumgartner, H. (2006). Hemodynamic assessment of aortic stenosis: are there still lessons to learn? *J Am Coll Cardiol* 47(1), 138-140.

Chandra, S., N. M. Rajamannan and P. Sucosky (2012). Computational assessment of bicuspid aortic valve wall-shear stress: implications for calcific aortic valve disease. *Biomech Model Mechanobiol* 11(7), 1085-1096.

Chrisohoides, A. and F. Sotiropoulos (2003). Experimental visualization of Lagrangian coherent structures in aperiodic flows. *Physics of Fluids* 15(3), L25-L28.

DeGroff, C. G. (2002). Doppler echocardiography. *Pediatr Cardiol* 23(3), 307-333.

Gnyaneshwar, R., R. K. Kumar and K. R. Balakrishnan (2002). Dynamic analysis of the aortic valve using a finite element model. *The Annals of Thoracic Surgery* 73(4), 1122-1129.

Haller, G. and G. Yuan (2000). Lagrangian coherent structures and mixing in two-dimensional turbulence. *Physica D: Nonlinear Phenomena* 147(3–4), 352-370.

Kuan, M. Y. and D. M. Espino (2015). Systolic fluid-structure interaction model of the

congenitally bicuspid aortic valve: assessment of modelling requirements. *Comput Methods Biomech Biomed Engin* 18(12), 1305-1320.

Maleki, H., S. Shahriari, L. G. Durand, M. R. Labrosse and L. Kadem (2014). A metric for the stiffness of calcified aortic valves using a combined computational and experimental approach. *Medical & Biological Engineering & Computing* 52(1), 1-8.

Mei, S., F. S. de Souza Junior, M. Y. Kuan, N. C. Green and D. M. Espino (2016). Hemodynamics through the congenitally bicuspid aortic valve: a computational fluid dynamics comparison of opening orifice area and leaflet orientation. *Perfusion*.

Olcay, A. B. (2016). Investigation of a wake formation for flow over a cylinder using Lagrangian coherent structures. *Progress in Computational Fluid Dynamics, an International Journal* 16(2), 126-130.

Olcay, A. B. and P. S. Krueger (2008). Measurement of ambient fluid entrainment during laminar vortex ring formation. *Experiments in Fluids* 44(2), 235-247.

Olcay, A. B. and P. S. Krueger (2010). Momentum evolution of ejected and entrained fluid during laminar vortex ring formation. *Theoretical and Computational Fluid Dynamics* 24(5): 465-482.

Pan, Y., A. Qiao and N. Dong (2015). Fluid–Structure Interaction Simulation of Aortic Valve Closure with Various Sinotubular Junction and Sinus Diameters. *Annals of Biomedical Engineering* 43(6), 1363-1369.

Shadden, S. C. and A. Arzani (2015). Lagrangian postprocessing of computational hemodynamics. *Ann Biomed Eng* 43(1), 41-58.

Shadden, S. C. and C. A. Taylor (2008). Characterization of Coherent Structures in the Cardiovascular System. *Annals of Biomedical Engineering* 36(7), 1152-1162.

Shadden, S. C., F. Lekien and J. E. Marsden (2005). Definition and properties of Lagrangian coherent structures from finite-time Lyapunov exponents in two-dimensional aperiodic flows. *Physica D: Nonlinear Phenomena* 212(3–4), 271-304.

Shadden, S. C., M. Astorino and J. F. Gerbeau (2010). Computational analysis of an aortic valve jet with Lagrangian coherent structures. *Chaos* 20(1), 017512.

Stewart, B. F., D. Siscovick, B. K. Lind, J. M. Gardin, J. S. Gottdiener, V. E. Smith, D. W. Kitzman and C. M. Otto (1997). Clinical factors associated with calcific aortic valve disease. *Cardiovascular Health Study. J Am Coll Cardiol* 29(3), 630-634.

Töger, J., M. Kanski, M. Carlsson, S. J. Kovács, G. Söderlind, H. Arheden and E. Heiberg (2012). Vortex Ring Formation in the Left Ventricle of the Heart: Analysis by 4D Flow MRI and Lagrangian Coherent Structures. *Annals of Biomedical Engineering* 40(12), 2652-2662.

Vétel, J., A. Garon and D. Pelletier (2009). Lagrangian coherent structures in the human carotid artery bifurcation. *Experiments in Fluids* 46(6), 1067-1079.

Weinberg, E. J., F. J. Schoen and M. R. K. Mofrad (2009). A Computational Model of Aging and Calcification in the Aortic Heart Valve. *PLOS ONE* 4(6), e5960.

Youssefi, P., A. Gomez, T. He, L. Anderson, N. Bunce, R. Sharma, C. A. Figueroa and M. Jahangiri (2017). Patient-specific computational fluid dynamics—assessment of aortic hemodynamics in a spectrum of aortic valve pathologies. *The Journal of Thoracic and Cardiovascular Surgery* 153(1), 8-20.